On the wave propagation characteristics of functionally graded porous shells using high-order shear deformation theory

Saeed I. Tahir[1], Ismail M. Mudhaffar[1], Abdelouahed Tounsi[1,2*], Mohammed A. Al-Osta[1], Abdelbaki Chikh[3,4]

[1] King Fahd University of Petroleum & Minerals, Dhahran, Saudi Arabia
[2]Lebanese American University, Byblos, Lebanon
[3]University of Sidi Bel Abbes, Algérie
[4]Université Ibn Khaldoun, Algérie
[*]Corresponding author: tou_abdel@yahoo.com

ARTICLE INFO

DOI:10.46223/HCMCOUJS.acs.en.14.1.152.2024

Received: September 3rd, 2023
Revised: November 28th, 2023
Accepted: December 15th, 2023

Keywords:
FGM shell; HSDT; porosity; wave propagation

ABSTRACT

This paper concentrates on the wave propagation characteristics of Functionally Graded (FG) porous shells. The transversal shear deformation of the shell is taken into consideration by employing a simple higher-ordered shear deformation shell theory. The equations of motion are derived for the proposed model based on Hamilton's principle. An eigenvalue problem that relates the wave propagation elements is formulated and solved to present the various dispersion relations of FG cylindrical and spherical shells. The effects of porosities, shells' geometrical parameters, FG material exponent, and wavenumbers on the principal wave propagation frequency and the associated phase velocity are investigated in detail. The research reveals that the phase velocities of waves traversing through shells are predominantly influenced by the porosity and the thickness and gradation of the constituent materials, whereas the geometric configuration of the shells, whether cylindrical or spherical, exerts a negligible impact.

1. Introduction

A civilization's backbone is its structure. Over time, structures' designs are evolving, improving the materials, geometry, and design methods. Initially, the materials used in manufacturing were homogeneous, causing deficiencies. Understanding composite laminated materials was the result. Even so, stress concentration occurs on the interfaces of the layers, leading to delamination, cracks, and other damage mechanisms such as out-of-plane and in-plane shear. A new generation of materials, Functionally Graded Materials (FGMs), overcome these deficiencies by carefully varying the component materials throughout the thickness, serving a specific function; hence their name. Structures made from FGM are typically made from ceramics and metals. Because the ceramic phase has a low thermal conductivity, it provides elevated temperature resistance, whereas the ductile metal phase prevents fracture caused by rising temperatures in a noticeably brief time. Furthermore, A FGM's superior characteristics make it suitable for use in many fields, such as civil, mechanical, nuclear, etc. With FGMs, engine parts for airplanes and cars, rocket launchpads, submarine bodies, and hard-cutting tools can all be designed efficiently.

Beams, plates, and shells are the most common FGM structures. A shell is identified by two parameters associated with the shell's curvature. The types of curvatures determine the type of shell, such as elliptical, circular, conical, etc. Scientists have studied the bending, vibration, and buckling responses of shells, leading to an abundance of theory development. The 3D elasticity method is mathematically complex and computationally costly, igniting the need for simpler 2D theories. These theories are combined into three main categories. First, the Classical Shell Theory

(CST) was first used by Aron (1874) and later corrected by Love (1888). The CST neglects the transverse shear and captures the response of thin shells. However, thick shells require theories that take into consideration the effect of the transverse shear. Second is the First-Order shear deformation theory (FOSDT), in which Mindlin (1951) included the transverse shear strain effect. However, shear correction factors are required to ensure zero shear tresses at the top and bottom of the plates. The third type is the Higher-order shear deformation theory (HSDT), in which the displacement field is expressed in three terms accounting for transverse shear strain and no need for shear correction factors.

The above-mentioned theories have been utilized in an abundance of articles to investigate shell bending and vibrational response. Liu, Wang, Wang, and Qin (2020) investigated the free vibration of FGM cylindrical shells using the FSDT while including an expansion of the wave function in the displacement field. By using the Wave-Based Method (WBM), the boundary conditions of the shell could be arbitrarily defined while maintaining the ease of construction of the global matrix. Hua, You, Huang, Fu, and Zhou (2024) studied the wave propagation of cracked cylindrical shells using the spectral element method and the first-order shear deformation theory. Tornabene (2009) presented a generalized differential quadrature solution based on first-order shear distribution theory to study the dynamic behavior of moderately thick, functionally graded conical, cylindrical, and annular plates. Using a modified First-order Shear Deformation Theory (FSDT), Mellouli, Jrad, Wali, and Dammak (2019) investigated the meshless implementation of arbitrary 3D-shell structures. Assuming a parabolic distribution of shear strain in the FSDT corrected the constant shear stress in the Mindlin-Reissner theory. Thus, the shear strain distribution through thickness was closer to a realistic distribution. As a part of Su and Jin's (2016) research, spectral element analysis is used to analyze the free vibration of conical, cylindrical, and spherical shells with arbitrary boundary conditions. Every segment of the compound shell system is formulated using the first-order shear deformation shell theory. Several cases were considered, such as cylindrical-conical and cylindrical-spherical shells. Shahbaztabar, Izadi, Sadeghian, and Kazemi (2019) investigated the free vibration problem of circular, functionally graded, circularly cylinder shells embedded in a Pasternak elastic foundation and partially or completely in contact with a fluid based on the first-order shear deformation theory. Using the first-order shear deformation shell theory, Li (2019) determined the frequencies of stepped cylindrical shells. A multi-segment partitioning strategy is used for developing the analytical model. The Rayleigh-Ritz method is applied to obtain the solution to the free vibration behavior of FG cylindrical shells. Tornabene, Fantuzzi, and Bacciocch (2014) used higher order equivalent layer theory with Mukurami zigzag function effects to study the free vibration behavior of free-form doubly curved FG shells. Mori Tanaka's model of material gradation has been used to solve equations using the GDQ method. In their study, Punera, Kant, and Desai (2018) use a higher-order theory to investigate the response of FG sandwich cylindrical shells considering both shear and normal strain effects. An extended thickness criterion is proposed as well, which makes the theory more applicable to thick and moderately thick shells.

Some voids or pores exist in the functionally graded material during the production process because of processing defects. Such porosities influence the structure's static and dynamic responses. Analytical investigations were performed by Fu, Wu, Xiao, and Chen (2020) on Porous Functionally Graded Material (P-FGM) cylindrical shells placed on elastic foundations under nonlinear thermal conditions. Three common types of PFGM cylindrical shells were considered based on the nonlinear heat conduction equation: uniform, symmetric, and asymmetric. The material properties were assumed to be dependent on temperature. Using blast loads and thermal conditions, Karakoti, Pandey, and Kar (2022) examined nonlinear transients of porous P-FGM and S-FGM sandwich plates and shell panels. A thin functionally graded cylindrical shell under uniform torsion was examined by Vu and Hoang (2022b) to determine its buckling and post-buckling behaviors under porosity and tangential constraints. To determine the effective properties

of porous FGM, the properties of constituencies were estimated according to a modified mixture rule. From a classical shell theory, mathematical forms were developed that consider von Kármán-Donnell's elasticity and nonlinearity. By applying Donnell shell theory to (PFGM) cylindrical shells, Timesli (2021) investigated their buckling behavior. Through a modified power-law function and the Winkler and Pasternak models, the author developed explicit analytical expressions that consider the effects of porosities through the thickness of the shell and the elastic foundation. To obtain the nonlinear equations of motion, Liu and Qin (2021) applied Donnell's nonlinear shallow shell theory and Hamilton's principle to sandwich cylindrical shells with porosities on an elastic substrate. Using uniform, symmetric, and asymmetric distributions and assuming that material properties are related to temperature, Fu, Wu, Xiao, and Chen (2021) presented a semi-analytical method to investigate the dynamic instability of (PFGM) conical shells in thermal environments. Recent articles on the effect of a shell's porosity include Foroutan and Dai (2022); Mirjavadi, Forsat, Barati, and Hamouda (2022); Le, Bui, Do, and Dang (2022a).

Furthermore, it has been possible to investigate the vibrations of shells with a variety of boundary conditions by researchers. In their research, Najafizadeh and Isvandzibaei (2007) investigated the vibration of a thin Functionally Graded (FG) cylindrical shell. The shell is graded with stainless steel and nickel resting on simply supported SS-SS boundary conditions with ring support in the axial direction. The free vibration of shells composed of two outer layers of homogenous materials and a middle layer of FGM was investigated by Li, Fu, and Batra (2010). The shell is simply supported, and the governing equations are derived using Flügge's shell theory. Using the system of joined shells made of FGM, Bagheri, Kiani, and Eslami (2021) studied the natural frequencies of conical and spherical shells. By assuming Donnel-type kinematics, the equations of motion are derived by assuming identical thickness for both shapes. Using the domain decomposition method, Wu, Qu, and Hua (2013) studied the free vibration of a joined cylindrical-spherical shell with elastic boundary conditions. Qu, Long, Yuan, and Meng (2013) studied vibration characteristics of FG cylindrical shells with general boundary conditions using Chebyshev polynomials of the first kind, Chebyshev polynomials of the second kind, and Legendre polynomials. Each of the three polynomials is orthogonal, complete, and has a simple form.

Additionally, researchers are concerned about the buckling and static responses of the shell. An extension of the Kirchhoff-Love model to the analysis of functionally graded structures during thermal buckling and post-buckling was carried out by Trabelsi, Zghal, and Dammak (2020). The delaminated region of a fiber-reinforced laminated cylindrical shell was modeled as an elliptical, triangular, or lemniscate shape by Wang, Lu, and Xiao (2002) to investigate the nonlinear thermal buckling behavior near the surface of fiber-reinforced laminated cylindrical shells near the surface. By applying the Galerkin method, the temperature distribution through the thickness direction was assumed by Sofiyev (2011) to be nonlinear in the case of thermal buckling of FGM circular truncated conical shells resting on two-parameter elastic foundations. Analyzing linear statics of composite structures reinforced with functionally rated carbon nanotubes was the purpose of a study by Zghal, Frikha, and Dammak (2017). Researchers considered five kinds of distributions of uniaxially aligned reinforcements along with the thickness of shell structures, i.e., one uniform and four functionally graded distributions. Recent articles on static and buckling analysis include Chang and Zhou (2022); Le, Pham, Bui, and Do (2022b); Talebi, Hedayati, Sadighi, and Ashoori (2022); Vu and Hoang (2022a).

Many recent articles experimentally and analytically investigated the static and dynamic behavior of porous shells. Ramteke and Panda (2023) used a higher-order theory to develop a finite element model investigating the dynamic and static response on porous shells which confirmed the experimental results as well as published results. Xue, Jin, Zhang, Han, and Chen (2023) used a first-order shear theory and various porosity distributions along the thickness and length of cylindrical shells to study their vibration response. The weak form obtained was solved using the isogeometric analysis method (IGA) and the findings revealed a significant influence of the

symmetry in porosity distribution on the mode shapes. The wave propagation induced by thermal strain energy in FG cylindrical shells was investigated by Liang, Yaw, and Lim (2023) using first-order shear deformation theory. It is worth noting that research is ongoing on shells reinforced with nanomaterials, for example, Zhang et al. (2022) investigated the propagation of waves on shells reinforced with carbon nanotubes using a nonlocal strain gradient model of a first-order theory.

In contrast, other theories of higher-order shells generate a host of unknowns. Their governing motion equations are more complicated and computationally expensive than the ones yielded by the present theory. Based on this theory, this work traces wave propagation analysis of functionally graded porous shells using only four unknowns and four governing motion equations, which is a problem not handled in any article before. In this paper, we introduce undetermined integral terms into the displacement field in order to develop a new formulation of the governing differential equations. This hypothesis aims to simplify the analytical solution of different and complex shell problems by reducing the order of derivatives and the number of unknowns. The equations of motion are derived using Hamilton's principle. Navier's method is used to derive closed-form analytical solutions. With this theory, both shear strains and stresses are addressed in a hyperbolic way, ensuring that the top and bottom surfaces of the shell are stress-free.

2. FGM shell configuration

This section indicates a summary of theories/theoretical points/research that have been conducted previously. On that basis, propose research models, research hypotheses, or analytical frameworks.

Consider a shell with a ceramic outer surface and a metallic inner surface with a ceramic-metal functionally graded composition in between, as shown in Figure 1. The spherical shell (on the left) has a curvature in two directions, with radii R_1 and R_2. The cylindrical shell (in the right) has a curvature in a single direction while R_2 approaches infinity.

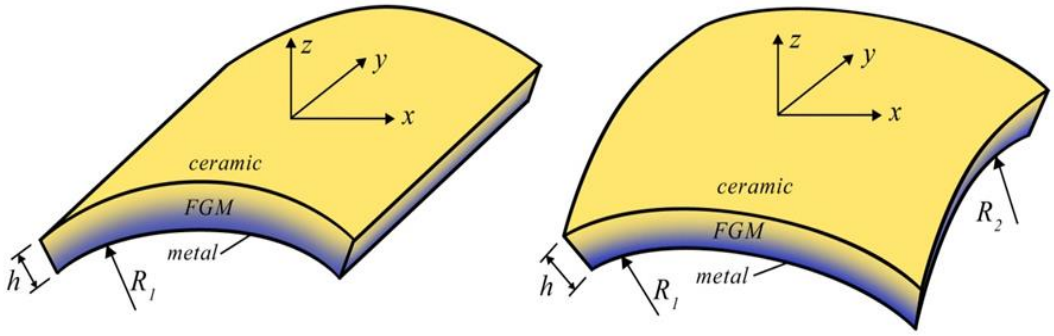

Figure 1. Figure caption Geometries and coordinate systems for FGM cylindrical and spherical shells

A continuous variation in the volume fraction of ceramic and metal constituents can easily be produced by manufacturing a mixture of these materials. Consequently, a power-law distribution can be used to express the volume fractions of the ceramic V_c and metal V_m phases as follows:

$$E(z) = E_m + (E_c - E_m)V_c - \lambda/2\ (E_c + E_m)$$
$$\rho(z) = \rho_m + (\rho_c - \rho_m)V_c - \lambda/2\ (\rho_c + \rho_m) \quad (1)$$

where the ceramic volume fraction $(\mathrm{V_c})$ follows the power law given by

$$V_c = \left(\frac{2z - h}{2h}\right)^P \quad (2)$$

$\mathrm{E_c}$, $\mathrm{E_m}$, and $\mathrm{E(z)}$ are the ceramic, metal, and effective Young's moduli, respectively.

ρ_c, ρ_m, and $\rho(z)$ are the ceramic, metal, and effective mass densities. The Poisson's ratio (υ) is considered to be constant. λ is the volume fraction of the uniformly distributed porosities.

3. Formulation

3.1. Kinematics

The present analysis of the FG shell is based on the following displacement field.

$$u(x,y,z,t) = \left(1+\frac{z}{R_1}\right)u_0(x,y,t) - z\frac{\partial w}{\partial x} + k_1 f(z)\int \theta(x,y,t)\,dx$$

$$v(x,y,z,t) = \left(1+\frac{z}{R_2}\right)v_0(x,y,t) - z\frac{\partial w}{\partial y} + k_2 f(z)\int \theta(x,y,t)\,dy \tag{3}$$

$$w(x,y,z,t) = w_0(x,y,t)$$

Where u, v, and w represent the displacements of the shell toward the x, y, and z directions, respectively, at any location in the FG shell. The subscript (0) indicates the given displacement in the shell's mid-plane. These mid-plane displacements depend only on time the position in the orthogonal curvilinear coordinates (x, y), but they are independent of the z coordinate. The shear shape function $f(z)$ implemented in the present analysis has a hyperbolic form given by Belabed et al. (2021).

$$f(z) = \frac{cosh\left(\frac{\pi}{2}\right)h^2\left(z\pi\, cosh\left(\frac{\pi}{2}\right) - h\, sinh\left(\frac{\pi z}{h}\right)\right)}{\frac{\pi}{2}\left(cosh\left(\frac{\pi}{2}\right)-1\right)} \tag{4}$$

The linear strain components obtained from the present HSDT are separated based on the z-dependent coefficient in each term and simplified as follows.

$$\begin{Bmatrix}\varepsilon_x\\ \varepsilon_y\\ \gamma_{xy}\end{Bmatrix} = \begin{Bmatrix}\varepsilon_x^0\\ \varepsilon_y^0\\ \gamma_{xy}^0\end{Bmatrix} - z\begin{Bmatrix}\varepsilon_x^b\\ \varepsilon_y^b\\ \gamma_{xy}^b\end{Bmatrix} + f(z)\begin{Bmatrix}\varepsilon_x^s\\ \varepsilon_y^s\\ \gamma_{xy}^s\end{Bmatrix}, \qquad \begin{Bmatrix}\gamma_{xz}\\ \gamma_{yz}\end{Bmatrix} = \frac{df(z)}{dz}\begin{Bmatrix}\gamma_{xz}^s\\ \gamma_{yz}^s\end{Bmatrix} \tag{5}$$

Where

$$\begin{Bmatrix}\varepsilon_x^0\\ \varepsilon_y^0\\ \gamma_{xy}^0\end{Bmatrix} = \begin{Bmatrix}\frac{\partial u_0}{\partial x}+\frac{w_0}{R_1}\\ \frac{\partial v_0}{\partial y}+\frac{w_0}{R_2}\\ \frac{\partial u_0}{\partial y}+\frac{\partial v_0}{\partial x}\end{Bmatrix}, \qquad \begin{Bmatrix}\varepsilon_x^b\\ \varepsilon_y^b\\ \gamma_{xy}^b\end{Bmatrix} = \begin{Bmatrix}\frac{\partial^2 w_0}{\partial x^2}\\ \frac{\partial^2 w_0}{\partial y^2}\\ 2\frac{\partial^2 w_0}{\partial x \partial y}\end{Bmatrix}, \tag{6}$$

$$\begin{Bmatrix}\varepsilon_x^s\\ \varepsilon_y^s\\ \gamma_{xy}^s\end{Bmatrix} = \begin{Bmatrix}k_1\theta\\ k_2\theta\\ k_1\int\frac{\theta}{\partial y}dx + k_2\int\frac{\theta}{\partial x}dy\end{Bmatrix}, \qquad \begin{Bmatrix}\gamma_{xz}^s\\ \gamma_{yz}^s\end{Bmatrix} = \begin{Bmatrix}k_1\int\theta\,dx\\ k_2\int\theta\,dy\end{Bmatrix}$$

The undetermined integral of θ is equivalent to the following forms:

$$\int\theta\,dx = A'\frac{\partial\theta}{\partial x}\,, \int\theta\,dy = B'\frac{\partial\theta}{\partial y} \tag{7}$$

Where, A', B', k_1 and k_2 are given by Tahir et al. (2022):

$$A' = -\frac{1}{\kappa_1^2}\,, B' = -\frac{1}{\kappa_2^2}\,, k_1 = \kappa_1^2\,, k_2 = \kappa_2^2 \tag{8}$$

Based on the defined strains, the stresses of FG shells are obtained via the constitutive relations.

$$\begin{Bmatrix} \sigma_x \\ \sigma_y \\ \tau_{xy} \\ \tau_{yz} \\ \tau_{xz} \end{Bmatrix} = \begin{bmatrix} Q_{11} & Q_{12} & 0 & 0 & 0 \\ Q_{12} & Q_{22} & 0 & 0 & 0 \\ 0 & 0 & Q_{66} & 0 & 0 \\ 0 & 0 & 0 & Q_{44} & 0 \\ 0 & 0 & 0 & 0 & C_{Q_{55}} \end{bmatrix} \begin{Bmatrix} \varepsilon_x \\ \varepsilon_y \\ \gamma_{xy} \\ \gamma_{xz} \\ \gamma_{yz} \end{Bmatrix} \tag{9}$$

Where the coefficients Q_{ij} are defined by:

$$Q_{11} = Q_{22} = \frac{E(z)}{1-\nu^2}\,, Q_{12} = \frac{\nu\, E(z)}{1-\nu^2}$$
$$Q_{44} = Q_{55} = Q_{66} = \frac{E(z)}{2\nu+2} \tag{10}$$

3.2. Governing equations

The equations are derived by employing the Hamilton principle.

$$\int_0^t (\delta U + \delta V - \delta K)\, dt = 0 \tag{11}$$

U, V, and K are the internal energy, the external work done on the shell, and the kinetic energy, respectively, and the first variation operator I denoted by δ. The variation of the shell's internal energy is given by:

$$\begin{aligned} \delta U = \int_\Omega \big(& N_x \delta\varepsilon_x^0 + N_y \delta\varepsilon_y^0 + N_{xy}\delta\gamma_{xy}^0 + M_x^b \delta\varepsilon_x^b + M_y^b \delta\varepsilon_y^b + M_{xy}^b \delta\varepsilon_{xy}^b + M_x^s \delta\varepsilon_x^s + M_y^s \delta\varepsilon_y^s \\ & + M_{xy}^s \delta\varepsilon_{xy}^s + S_{xz}\delta\gamma_{xz}^0 + S_{yz}\delta\gamma_{yz}^s \big)\, d\Omega \end{aligned} \tag{12}$$

where Ω outer surface of the shell, and N_i, M_i^j, and S_i are the internal resultant forces and moments that are defined for the FGM porous shell by:

$$\begin{bmatrix} N_x & N_y & N_{xy} \\ M_x^b & M_y^b & M_{xy}^b \\ M_x^s & M_y^s & M_{xy}^s \end{bmatrix} = \sum_{n=1}^{3} \int_{h_{n-1}}^{h_n} \begin{Bmatrix} 1 \\ z \\ f(z) \end{Bmatrix} . (\sigma_x, \sigma_y, \tau_{xy}) dz \tag{13}$$

and

$$\begin{Bmatrix} S_{xz} \\ S_{yz} \end{Bmatrix} = \sum_{n=1}^{3} \int_{h_{n-1}}^{h_n} g(z) \begin{Bmatrix} \tau_{xz} \\ \tau_{yz} \end{Bmatrix} dz \tag{14}$$

The resultant forces can be expressed in terms of the strain components as follows:

$$\begin{Bmatrix} N_x \\ N_y \\ M_x^b \\ M_y^b \\ M_x^s \\ M_y^s \end{Bmatrix} = \begin{bmatrix} A_{11} & A_{12} & B_{11} & B_{12} & B_{11}^s & B_{12}^s \\ A_{12} & A_{22} & B_{12} & B_{22} & B_{12}^s & B_{22}^s \\ B_{11} & B_{12} & D_{11} & D_{12} & D_{11}^s & D_{12}^s \\ B_{12} & B_{22} & D_{12} & D_{22} & D_{12}^s & D_{22}^s \\ B_{11}^s & B_{12}^s & D_{11}^s & D_{12}^s & H_{11}^s & H_{12}^s \\ B_{12}^s & B_{22}^s & D_{12}^s & D_{22}^5 & H_{12}^s & H_{22}^s \end{bmatrix} \begin{Bmatrix} \varepsilon_x^0 \\ \varepsilon_y^0 \\ \varepsilon_x^b \\ \varepsilon_y^b \\ \varepsilon_x^s \\ \varepsilon_y^s \end{Bmatrix}, \tag{15}$$

$$\begin{Bmatrix} N_{xy} \\ M_{xy}^{b} \\ M_{xy}^{s} \end{Bmatrix} = \begin{bmatrix} A_{66} & B_{66} & B_{66}^{s} \\ B_{66} & D_{66} & D_{66}^{s} \\ B_{66}^{s} & D_{66}^{s} & H_{66}^{s} \end{bmatrix} \begin{Bmatrix} \gamma_{xy}^{0} \\ \gamma_{xy}^{b} \\ \gamma_{xy}^{s} \end{Bmatrix},$$

$$\begin{Bmatrix} S_{xz} \\ S_{yz} \end{Bmatrix} = \begin{bmatrix} A_{44}^{s} & 0 \\ 0 & A_{55}^{s} \end{bmatrix} \begin{Bmatrix} \gamma_{xz}^{s} \\ \gamma_{yz}^{s} \end{Bmatrix}$$

Where

$$\begin{bmatrix} A_{11} & B_{11} & B_{11}^{s} & D_{11} & D_{11}^{s} & H_{11}^{s} \\ A_{22} & B_{22} & B_{22}^{s} & D_{22} & D_{22}^{s} & H_{22}^{s} \\ A_{12} & B_{12} & B_{12}^{s} & D_{12} & D_{12}^{s} & H_{12}^{s} \\ A_{66} & B_{66} & B_{66}^{s} & D_{66} & D_{66}^{s} & H_{66}^{s} \end{bmatrix} = \sum_{n=1}^{3} \int_{h_{n-1}}^{h_n} (1, z, f, z^2, zf, f^2) \begin{Bmatrix} Q_{11} \\ Q_{22} \\ Q_{12} \\ Q_{66} \end{Bmatrix} dz \tag{16}$$

and

$$\begin{Bmatrix} A_{44}^{s} \\ A_{55}^{s} \end{Bmatrix} = \sum_{n=1}^{3} \int_{h_{n-1}}^{h_n} g(z)^2 \begin{Bmatrix} Q_{44} \\ Q_{55} \end{Bmatrix} dz \tag{17}$$

The external work is zero since the FGM shell is considered to be not under any external forces. The variation of the kinetic energy is given by:

$$\begin{aligned} \delta K = \int_A \Bigg(& \left(I_0 + \frac{2I_1}{R_1}\right)\ddot{u}_0 - \left(I_1 + \frac{I_3}{R_1}\right)\frac{\partial \ddot{w}_0}{\partial x} + \left(I_2 + \frac{I_4}{R_1}\right)k_1 A' \frac{\partial \ddot{\theta}}{\partial x} \Bigg) \delta u_0 \\ & + \left(\left(I_0 + \frac{2I_1}{R_2}\right)\ddot{v}_0 - \left(I_1 + \frac{I_3}{R_2}\right)\frac{\partial \ddot{w}_0}{\partial y} + \left(I_2 + \frac{I_4}{R_2}\right)k_2 B' \frac{\partial \ddot{\theta}}{\partial y} \right) \delta v_0 \\ & + \Bigg(-\left(I_1 + \frac{I_3}{R_1}\right)\frac{\partial \ddot{u}_0}{\partial x} + I_3 \frac{\partial^2 \ddot{w}_0}{\partial x^2} - I_4 k_1 A' \frac{\partial^2 \ddot{\theta}}{\partial x^2} - \left(I_1 + \frac{I_3}{R_2}\right)\frac{\partial \ddot{v}_0}{\partial y} \\ & + I_3 \frac{\partial^2 \ddot{w}_0}{\partial y^2} - I_4 k_2 B' \frac{\partial^2 \ddot{\theta}}{\partial y^2} + I_0 \ddot{w}_0 \Bigg) \delta w_0 \\ & + \Bigg(k_1 A' \left(I_2 + \frac{I_4}{R_1}\right)\frac{\partial \ddot{u}_0}{\partial x} - I_4\, k_1 A' \frac{\partial^2 \ddot{w}_0}{\partial x^2} + I_5 (k_1 A')^2 \frac{\partial^2 \ddot{\theta}}{\partial x^2} \\ & + k_2 B' \left(I_2 + \frac{I_4}{R_2}\right)\frac{\partial \ddot{v}_0}{\partial y} - I_4\, k_2 B' \frac{\partial^2 \ddot{w}_0}{\partial y^2} \\ & + I_5 (k_2 B')^2 \frac{\partial^2 \ddot{\theta}}{\partial y^2} \Bigg) \delta\theta \, dA \end{aligned} \tag{18}$$

Where

$$(I_0, I_1, I_2, I_3, I_4, I_5) = \sum_{n=1}^{3} \int_{h_{n-1}}^{h_n} (1, z, f, z^2, zf, f^2)\, \rho(z)\, dz \tag{19}$$

Using the derived expressions of δU and δK, the governing differential equations of the functionally graded shell are derived from the Hamilton principle to be:

$$\begin{aligned} \delta u_0 : \quad & \frac{\partial N_x}{\partial x} + \frac{\partial N_{xy}}{\partial y} = -\left(I_0 + \frac{2I_1}{R_1}\right)\ddot{u}_0 + \left(I_1 + \frac{I_3}{R_1}\right)\frac{\partial \ddot{w}_0}{\partial x} - k_1 A' \left(I_2 + \frac{I_4}{R_1}\right)\frac{\partial \ddot{\theta}}{\partial x} \\ \delta v_0 : \quad & \frac{\partial N_y}{\partial y} + \frac{\partial N_{xy}}{\partial x} = -\left(I_0 + \frac{2I_1}{R_2}\right)\ddot{v}_0 + \left(I_1 + \frac{I_3}{R_1}\right)\frac{\partial \ddot{w}_0}{\partial y} - k_2 B' \left(I_2 + \frac{I_4}{R_2}\right)\frac{\partial \ddot{\theta}}{\partial y} \end{aligned} \tag{20}$$

$$\delta w_0: \ \frac{\partial^2 M_X^b}{\partial x^2} + 2\frac{\partial^2 M_{xy}^b}{\partial x \partial y} + \frac{\partial^2 M_y^b}{\partial y^2} - \frac{N_x}{R_1} - \frac{N_y}{R_2}$$
$$= \left(I_1 + \frac{I_3}{R_1}\right)\frac{\partial \ddot{u}_0}{\partial x} - I_3\frac{\partial^2 \ddot{w}_0}{\partial x^2} + I_4 k_1 A'\frac{\partial^2 \ddot{\theta}}{\partial x^2} - \left(I_1 + \frac{I_3}{R_2}\right)\frac{\partial \ddot{v}_0}{\partial y}$$
$$- I_3\frac{\partial^2 \ddot{w}_0}{\partial y^2} + I_4 k_2 B'\frac{\partial^2 \ddot{\theta}}{\partial y^2} - I_0 \ddot{w}_0$$

$$\delta\theta: \ -A' k_1\frac{\partial^2 M_{xy}^s}{\partial x \partial y} - B' k_2\frac{\partial^2 M_{xy}^s}{\partial x \partial y} - k_1 M_x^s - k_2 M_y^s + A' k_1\frac{\partial S_{xz}}{\partial x} + B' k_2\frac{\partial S_{yz}}{\partial y}$$
$$= -k_1 A'\left(I_2 + \frac{I_4}{R_1}\right)\frac{\partial \ddot{u}_0}{\partial x} + I_4\, k_1 A'\frac{\partial^2 \ddot{w}_0}{\partial x^2} - I_5 (k_1 A')^2\frac{\partial^2 \ddot{\theta}}{\partial x^2}$$
$$- k_2 B'\left(I_2 + \frac{I_4}{R_2}\right)\frac{\partial \ddot{v}_0}{\partial y} + I_4\, k_2 B'\frac{\partial^2 \ddot{w}_0}{\partial y^2} - I_5 (k_2 B')^2\frac{\partial^2 \ddot{\theta}}{\partial y^2}$$

3.3. Dispersion relations

The general solution form of the present wave propagation problem is given as

$$\begin{Bmatrix} u_0(x,y,t) \\ v_0(x,y,t) \\ w_0(x,y,t) \\ \theta(x,y,t) \end{Bmatrix} = \begin{Bmatrix} U \\ V \\ W \\ \Theta \end{Bmatrix} exp\left[i(\kappa_1 x + \kappa_2 y - \omega t)\right] \tag{21}$$

U, V, W, and Θ are the wave amplitudes corresponding to the maximum displacements at a certain frequency ω. The motion equations are expressed in a matrix form after employing the solution form of wave propagation as follows:

$$([K] - \omega^2[M])\{\Lambda\} = 0 \tag{22}$$

Where $[K]$ is the stiffness matrix and $[M]$ is the mass matrix.

$$[K] = \begin{bmatrix} k_{11} & k_{12} & k_{13} & k_{14} \\ k_{12} & k_{22} & k_{23} & k_{24} \\ k_{13} & k_{23} & k_{33} & k_{34} \\ k_{14} & k_{24} & k_{34} & k_{44} \end{bmatrix}$$
$$[M] = \begin{bmatrix} m_{11} & 0 & m_{13} & m_{14} \\ 0 & m_{22} & m_{23} & m_{24} \\ m_{13} & m_{23} & m_{33} & m_{34} \\ m_{14} & m_{24} & m_{34} & m_{44} \end{bmatrix}, \{\Lambda\} = \begin{Bmatrix} U \\ V \\ W \\ \Theta \end{Bmatrix} \tag{23}$$

Where

$$k_{11} = A_{11}{\kappa_1}^2 + A_{66}{\kappa_2}^2$$
$$k_{12} = \kappa_1\kappa_2(A_{12} + A_{66})$$
$$k_{13} = -i\,\kappa_1\left(\frac{A_{11}}{R_1} + \frac{A_{12}}{R_2} + A\_12B_{11}\kappa_1^2 + \kappa_2^2(B_{12} + 2B_{66})\right)$$
$$k_{14} = -i\,\kappa_1(k_1 B_{11}^s + k_2 B_{12}^s - (A' k_1 + B' k_2)B_{66}^s\kappa_2^2) \tag{24}$$
$$k_{22} = A_{22}\kappa_2^2 + A_{66}\kappa_1^2$$
$$k_{23} = -i\,\kappa_2\left(\frac{A_{22}}{R_2} + \frac{A_{12}}{R_1} + B_{22}\kappa_2^2 + \kappa_1^2(B_{12} + 2B_{66})\right)$$

$$k_{24} = -i\,\kappa_2(k_2 B_{22}^s + k_1 B_{12}^s - (A'k_1 + B'k_2)B_{66}^s\kappa_1^2)$$

$$k_{33} = -\frac{A_{11}}{R_1^2} - \frac{A_{22}}{R_2^2} - \frac{2A_{12}}{R_1 R_2} - 2\left(\frac{B_{11}}{R_1} + \frac{B_{12}}{R_2}\right)\kappa_1^2 - 2\left(\frac{B_{22}}{R_2} + \frac{B_{12}}{R_1}\right)\kappa_2^2 - D_{11}{\kappa_1}^4 - D_{22}{\kappa_2}^4 - 2(D_{12} + 2D_{66}){\kappa_1}^2{\kappa_2}^2$$

$$k_{34} = -\left(\frac{B_{11}^s}{R_1} + \frac{B_{12}^s}{R_2}\right)k_1 - \left(\frac{B_{11}^s}{R_2} + \frac{B_{12}^s}{R_1}\right)k_2 - (k_1(D_{11}^s + k_2 D_{12}^s){\kappa_1}^2 - (k_1 D_{12}^s + k_2 D_{22}^s){\kappa_2}^2 + 2(A'k_1 D_{66}^s + B'k_2 D_{66}^s){\kappa_1}^2{\kappa_2}^2$$

$$k_{44} = -k_1^2 H_{11}^s - 2k_1 k_2 H_{12}^s - k_2^2 H_{22}^s - \left({A'}^2 k_1^2 + 2A'B'k_1 k_2 + {B'}^2 k_2^2\right)H_{66}^s\kappa_1^2\kappa_2^2 + A'k_1^2 A_{55}^s + B'k_2^2 A_{44}^s$$

and

$$\begin{aligned} m_{11} &= I_0 + 2I_1/R_1 \\ m_{13} &= -iI_1\kappa_1 - \kappa_1 I_3/R_1 \\ m_{14} &= iA'k_1 I_2\kappa_1 - (A'k_1\kappa_1)I_4/R_1 \\ m_{22} &= I_0 + 2I_1/R_2 \\ m_{23} &= -iI_1\kappa_2 + \kappa_2 I_3/R_2 \\ m_{24} &= iB'k_2 I_3\kappa_2 - (B'k_2\kappa_2)I_4/R_2 \\ m_{33} &= -I_0 - I_3({\kappa_1}^2 + {\kappa_2}^2) \\ m_{34} &= I_4(A'k_1{\kappa_1}^2 + B'k_2{\kappa_2}^2) \\ m_{44} &= -I_5((A'k_1\kappa_1)^2 + (B'k_2\kappa_2)^2) \end{aligned} \tag{25}$$

The principal frequencies are evaluated by solving the following eigenvalue problem.

$$|[K] - \omega^2[M]| = 0 \tag{26}$$

The phase velocity is related to the frequency by:

$$C_{ij} = \frac{\omega_j}{\kappa_i}, \quad (i = 1{,}2 \; and \; j = 1{,}2{,}3{,}4) \tag{27}$$

4. Result and discussion

This section illustrates how material exponent, porosity, and thickness affect wave propagation of FGM shells through various examples. The mechanical properties of ceramic and metal are $E_c = 380\,GPa$, $\rho_c = 3800\,kg/m^3$, $E_m = 70\,GPa$, $\rho_m = 2707\,kg/m^3$, and $v_c = v_m = 0.3$ (M. Sobhy, 2016). These properties are used to generate the following results along with $h = 0.1\,m$, $R = 5\,m$, $\kappa = 100\,m^{-1}$, $P = 1$, and $\lambda = 0.1$ as default values.

Figure 2 shows how varying the material power-law exponent affects the relationship between wavenumber (κ) and wave frequency (ω) for spherical and cylindrical shells. Wave frequencies are the same in spherical and cylindrical shells. In general, for both shapes, it is observed that the angular frequency of the wave decreases when the material is elevated from full ceramic ($P = 0$) to fully metal ($P = \infty$). In other words, the maximum frequency of a wave will occur in a ceramic shell, and it decreases in an FGM ceramic-metal shell, while the smallest frequency will occur when passing through a metal shell. Additionally, the angular frequency of

waves is proportional to their wavenumber for certain material exponents; the greater the wave number, the higher the frequency.

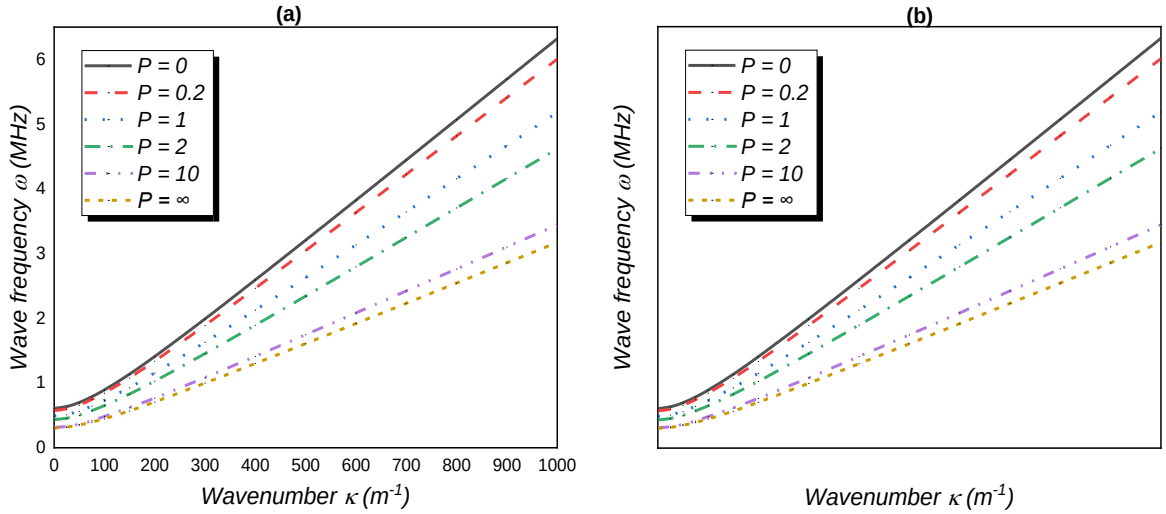

Figure 2. The dispersion relation between ω and κ of FG porous shells: (a) spherical shell, (b) cylindrical shell

The phase velocity (C) of a wave, on the other hand, is inversely proportional to the wavenumber; the higher the wavenumber, the lower the phase velocity. For low values of wavenumber ($\kappa < 300\ m^{-1}$), this relationship is very evident as the velocity tends to horizontally stabilize for higher values of wavenumber, as shown in Figure 3. The wave's phase velocity is also significantly lower when the material's power exponent is increased; the higher the metal's volume fraction, the lower the wave's phase velocity. This is explained by the lower density of metal $2707\ kg/m^3$ compared to that of the ceramic $3800\ kg/m^3$; compression and rarefaction are easier in denser materials.

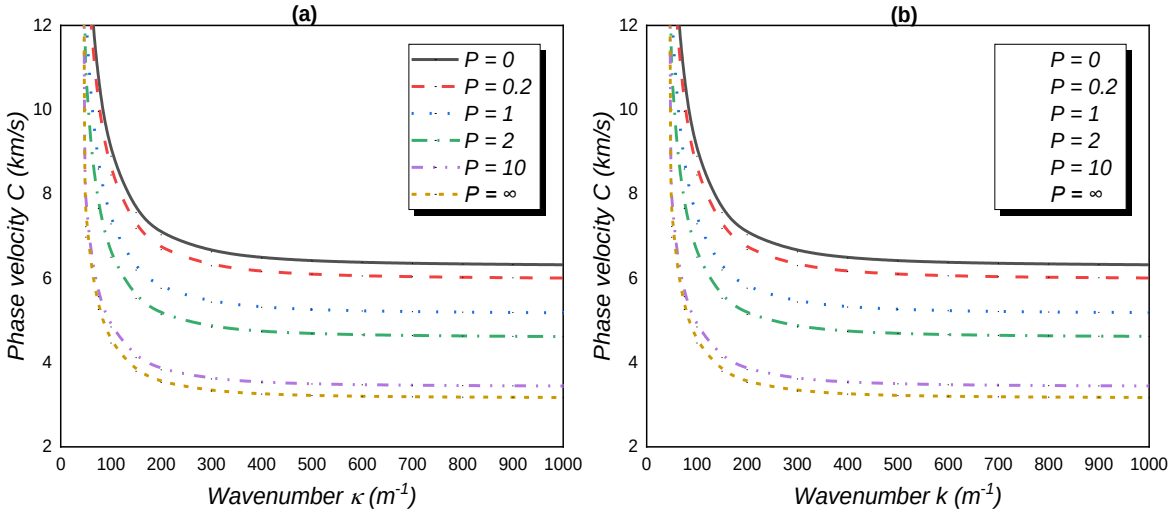

Figure 3. The dispersion relation between C and κ of FG porous shells: (a) spherical shell, (b) cylindrical shell

In Figure 4, the relationship between wave frequency and phase velocity is shown for various material exponents. Wave phase velocity decreases with increasing wave frequency regardless of the power exponent. More energy is transmitted to the medium in higher frequency waves, resulting in a slower speed. Likewise, as shown in Figure 3, shells with higher material exponents experience less velocity, and their shapes do not affect velocity.

As shown in Figures 5 and 6, shell thickness impacts phase velocity across the entire range of wavenumbers. The thicker the shell, the higher the phase velocity of the passing wave. It is

clear. However, that thickness has a significant impact on the velocity at low wavenumbers, while this effect becomes small at wavenumbers ($\kappa > 800\, m^{-1}$). A similar trend is noticed when considering the effect of the wave's frequency on the phase velocity, as shown in Figure 6. In the case of a particular wave frequency, thicker shells cause a higher velocity than thin shells. In addition, the lower phase velocity for a certain shell thickness is caused by large frequencies dissipating the kinetic energy of the wave. This is because large frequencies dissipate wave energy.

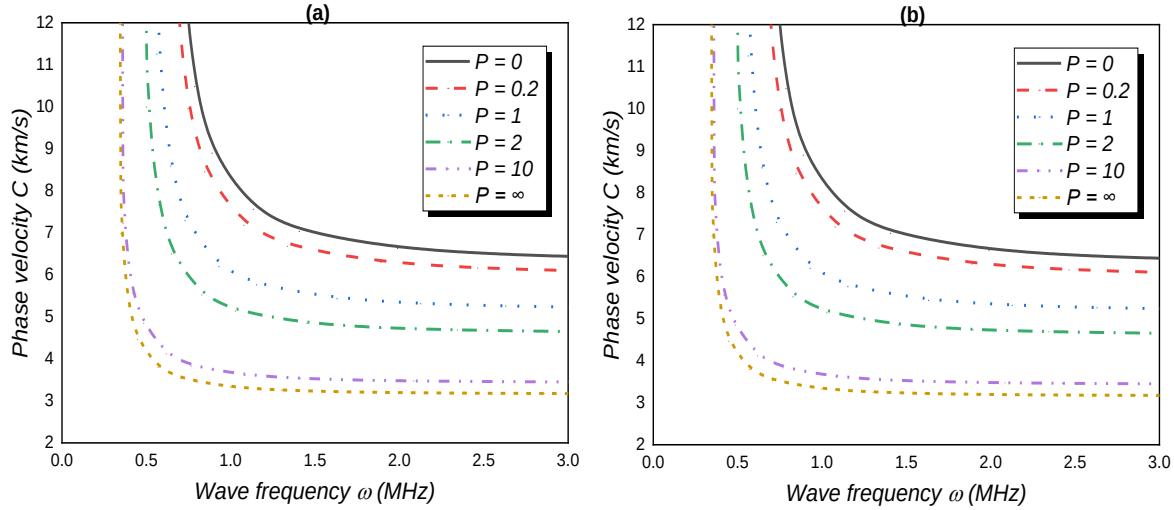

Figure 4. The dispersion relation between C and ω of FG porous shells: (a) spherical shell, (b) cylindrical shell

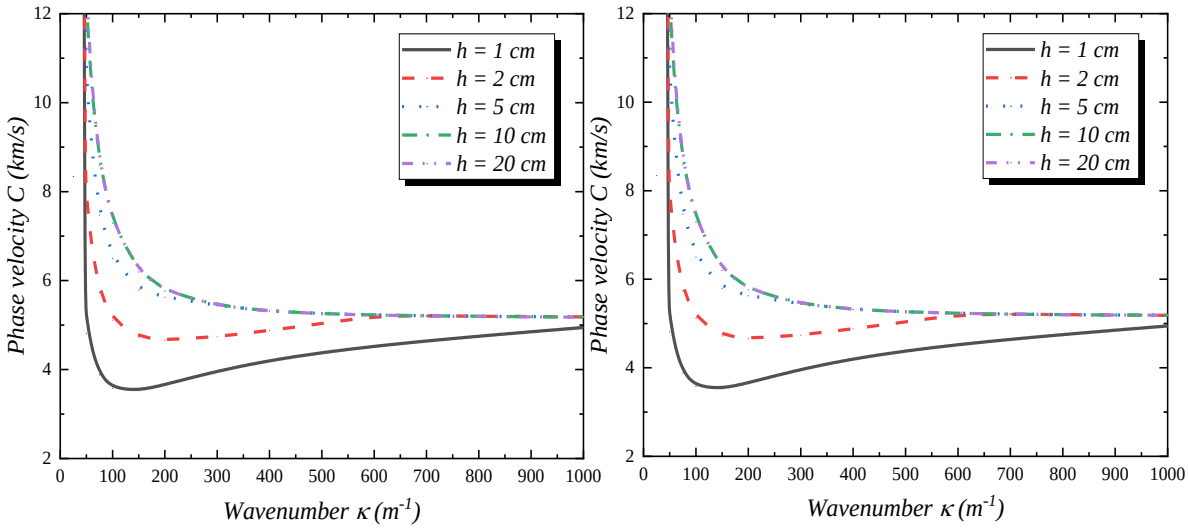

Figure 5. The dispersion relation between C and κ of FG porous shells: (a) spherical shell, (b) cylindrical shell

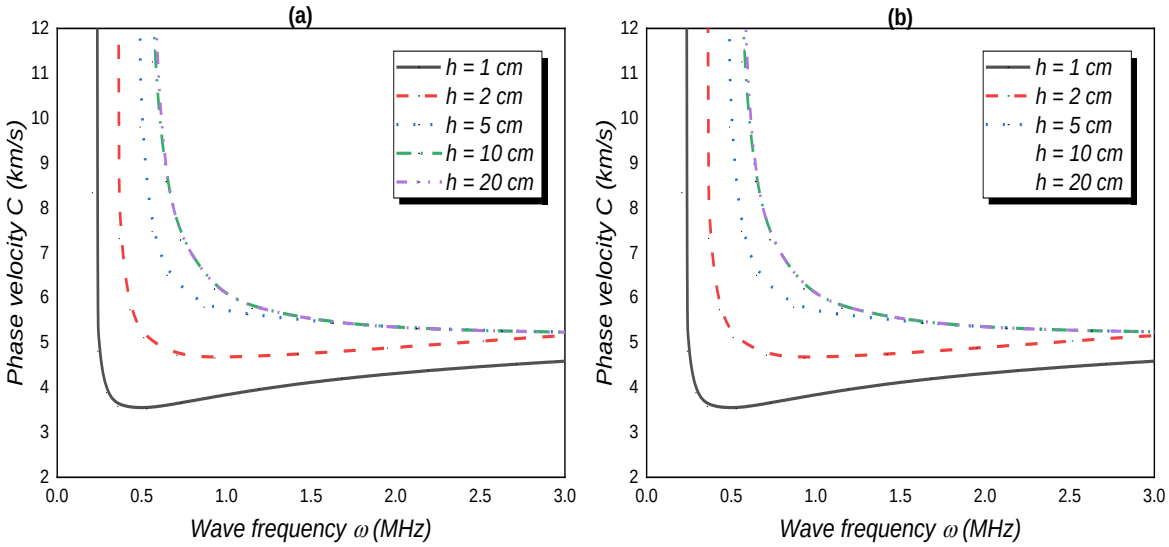

Figure 6. The dispersion relation between C and ω of FG porous shells: (a) spherical shell, (b) cylindrical shell

An examination of the effect of porosity volume fractions on the dispersion of waves in shells is shown in Figure 7. Having porosity decreases phase velocity, which is critical. When power exponents exceed one and porosity volume fractions exceed 0.2, there is a noticeable decrease in velocity. The effect is similar regardless of whether the shell is cylindrical or spherical.

A comparison of the shell thickness with the phase velocity is shown in Figure 8 for different radii of curvature. For all curvatures' radii, increasing the thickness leads to a slight velocity reduction. Shells with a spherical shape show a greater reduction than shells with a cylindrical shape.

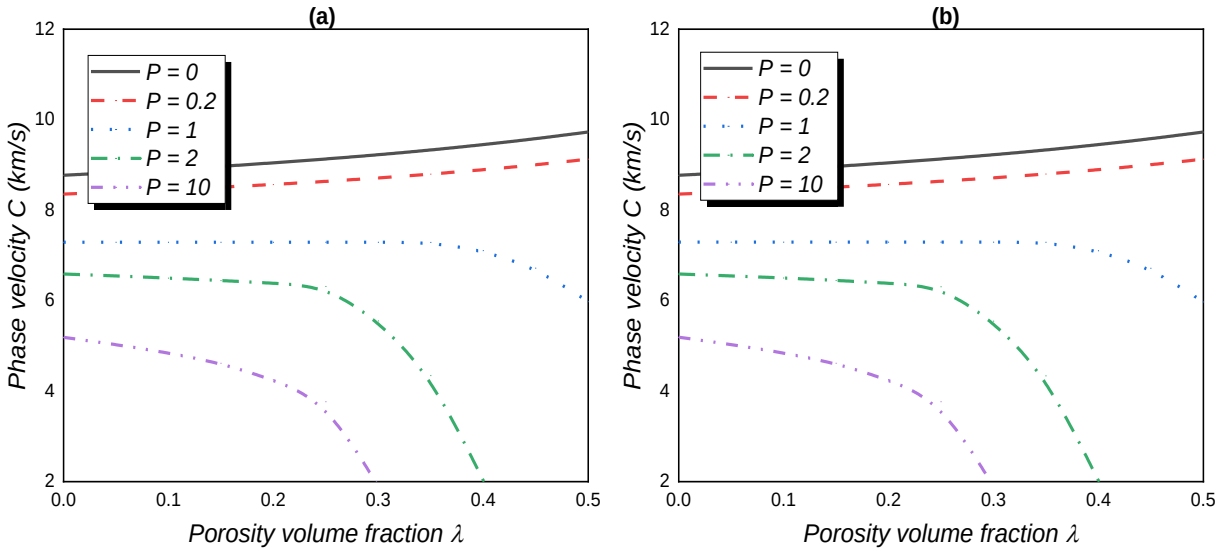

Figure 7. The dispersion relation between C and λ of FG porous shells: (a) spherical shell, (b) cylindrical shell

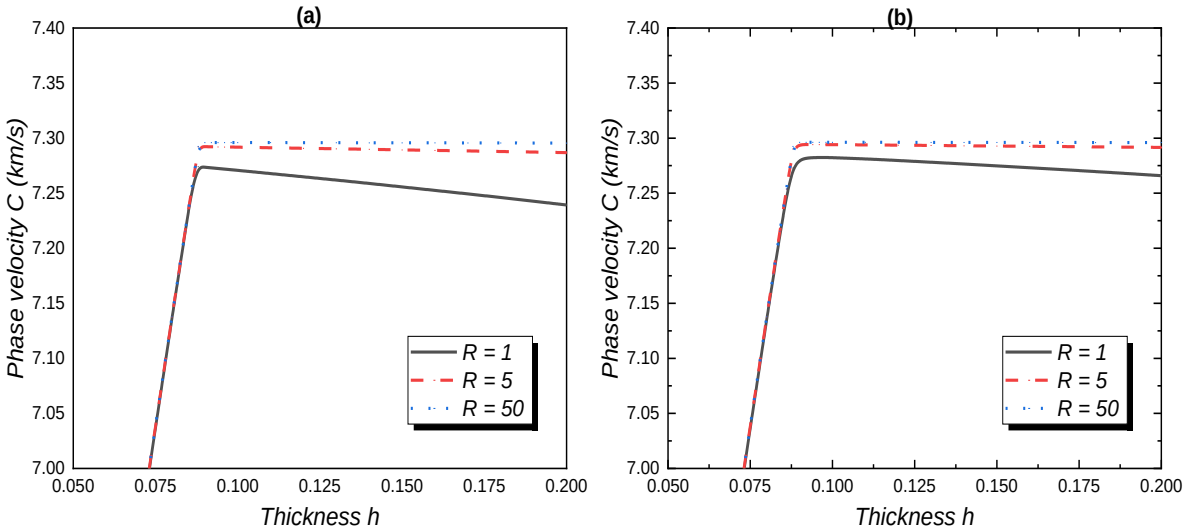

Figure 8. The dispersion relation between C and h of FG porous shells: (a) spherical shell, (b) cylindrical shell

As shown in Table 1, various parameters are investigated to determine the phase velocity of spherical shells, including the material exponents, the curvature radius, the thickness, the volume fraction, and the porosity. Generally, the phase velocity is proportional to curvature radii, thickness, and porosities but inversely proportional to material exponents. As shown in Table 2, the same investigation is conducted for cylindrical shells. By comparing the two tables, it is evident that the shape of the shell has a negligible effect on phase velocity. Consideration must be given, however, to porosities since their presence increases velocity values.

Table 1

Phase velocities (km/s) of FG porous spherical shells and flat panels for different material exponents, porosities volume fractions, thicknesses, and curvature radii ($R_1 = R_2 = R$)

R	**h**	**λ**	**P**					
			0	**0.2**	**1**	**2**	**10**	∞
10	0.05	0.00	07.981	07.584	06.533	05.830	04.514	04.062
		0.10	08.095	07.670	06.499	05.695	04.106	04.062
		0.20	08.230	07.773	06.444	05.480	03.476	04.062
		0.30	08.394	07.899	06.339	04.943	01.922	04.062
	0.10	0.00	08.771	08.355	07.294	06.590	05.191	04.464
		0.10	08.896	08.453	07.294	06.502	04.847	04.464
		0.20	09.045	08.570	07.294	06.387	04.252	04.464
		0.30	09.225	08.714	07.294	05.548	01.891	04.464
50	0.05	0.00	07.981	07.584	06.534	05.830	04.515	04.062
		0.10	08.095	07.670	06.500	05.696	04.106	04.062
		0.20	08.230	07.773	06.444	05.480	03.477	04.062
		0.30	08.394	07.899	06.340	04.943	01.921	04.062
	0.10	0.00	08.771	08.356	07.296	06.592	05.192	04.464

R	**h**	**λ**	**P**					
			0	**0.2**	**1**	**2**	**10**	∞
		0.10	08.896	08.454	07.296	06.503	04.848	04.464
		0.20	09.045	08.571	07.296	06.389	04.253	04.464
		0.30	09.225	08.715	07.296	05.542	01.889	04.464
∞	0.05	0.00	07.981	07.584	06.534	05.830	04.515	04.062
		0.10	08.095	07.670	06.500	05.696	04.106	04.062
		0.20	08.230	07.773	06.444	05.481	03.477	04.062
		0.30	08.394	07.899	06.340	04.943	01.921	04.062
	0.10	0.00	08.771	08.356	07.296	06.592	05.192	04.464
		0.10	08.896	08.454	07.296	06.504	04.848	04.464
		0.20	09.045	08.571	07.296	06.390	04.253	04.464
		0.30	09.225	08.715	07.296	05.541	01.888	04.464

Table 2

Phase velocities (km/s) of FG porous cylindrical shells for different material exponents, porosities volume fractions, thicknesses, and curvature radii ($R_2 = \infty$)

R_1	**h**	**λ**	**P**					
			0	**0.2**	**1**	**2**	**10**	∞
10	0.05	0.00	7.981	7.584	6.534	5.830	4.515	4.062
		0.10	8.095	7.670	6.500	5.695	4.106	4.062
		0.20	8.230	7.773	6.444	5.480	3.477	4.062
		0.30	8.394	7.899	6.340	4.943	1.921	4.062
	0.10	0.00	8.771	8.356	7.295	6.591	5.192	4.464
		0.10	8.896	8.453	7.295	6.503	4.848	4.464
		0.20	9.045	8.570	7.295	6.389	4.253	4.464
		0.30	9.225	8.714	7.295	5.544	1.890	4.464
50	0.05	0.00	7.981	7.584	6.534	5.830	4.515	4.062
		0.10	8.095	7.670	6.500	5.696	4.106	4.062
		0.20	8.230	7.773	6.444	5.481	3.477	4.062
		0.30	8.394	7.899	6.340	4.943	1.921	4.062
	0.10	0.00	8.771	8.356	7.296	6.592	5.192	4.464
		0.10	8.896	8.454	7.296	6.504	4.848	4.464
		0.20	9.045	8.571	7.296	6.390	4.253	4.464
		0.30	9.225	8.715	7.296	5.542	1.888	4.464

5. Conclusions

A four-unknown integral HSDT was used to investigate wave propagation in porous cylindrical and spherical shells. This study combines the advantages of reducing the number of variables to four, considering stretching of the thickness, and considering transverse shear. In this study, porosities have been shown to significantly influence the shell phase velocity, while the shape, whether cylindrical or spherical, had an insignificant effect. Additionally, the thickness and gradation of constituent materials were found to significantly influence the phase velocities of waves passing through the shells. The phase velocity is inversely proportional to the material exponent but proportional to the curvature radius, thickness, and porosity. It is important to note that this theory does not respect continuity conditions at interfaces between the layers, especially if laminated structures are used.

ACKNOWLEDGMENTS

The authors would like to acknowledge the support provided by the Interdisciplinary Research Center for Construction & Building Materials (IRC-CBM) at King Fahd University of Petroleum & Minerals (KFUPM), Saudi Arabia, for funding this work through Project No. INCB2209. The support provided by the Department of Civil & Environmental Engineering, KFUPM, Saudi Arabia, is also greatly acknowledged.

References

Aron, H. (1874). Das Gleichgewicht und die Bewegung einer unendlich dünnen, beliebig gekrümmten elastischen Schale. *Journal Für Die Reine und Angewandte Mathematik, 78*, 136-174.

Bagheri, H., Kiani, Y., & Eslami, M. R. (2021). Free vibration of FGM conical-spherical shells. *Thin-Walled Structures, 160*, Article 107387. doi:10.1016/j.tws.2020.107387

Belabed, Z., Selim, M. M., Slimani, O., Taibi, N., Tounsi, A., & Hussain, M. (2021). An efficient higher order shear deformation theory for free vibration analysis of functionally graded shells. *Steel and Composite Structures, 40*(2), 307-321. doi:10.12989/scs.2021.40.2.307

Chang, X., & Zhou, J. (2022). Static and dynamic characteristics of post-buckling of porous functionally graded pipes under thermal shock. *Composite Structures, 288*, Article 115373. doi:10.1016/j.compstruct.2022.115373

Do, C. Q., Tran, Q. Q., Bui, P. G., Dang, H. V., & Nguyen, D. D. (2022). Buckling analysis and dynamic response of FGM sandwich cylindrical panels in thermal environments using nonlocal strain gradient theory. *Acta Mech, 233*, 2213-2235. doi:10.1007/s00707-022-03212-8

Foroutan, K., & Dai, L. (2022). Nonlinear dynamic responses of porous FG sandwich cylindrical shells with a viscoelastic core resting on a nonlinear viscoelastic foundation. *Mechanics of Advanced Materials and Structures, 30*(15), 1-20. doi:10.1080/15376494.2022.2070803

Fu, T., Wu, X., Xiao, Z., & Chen, Z. (2020). Thermoacoustic response of porous FGM cylindrical shell surround by elastic foundation subjected to nonlinear thermal loading. *Thin-Walled Structures, 156*, Article 106996. doi:10.1016/j.tws.2020.106996

Fu, T., Wu, X., Xiao, Z., & Chen, Z. (2021). Dynamic instability analysis of porous FGM conical shells subjected to parametric excitation in thermal environment within FSDT. *Thin-Walled Structures, 158*, Article 107202. doi:10.1016/j.tws.2020.107202

Hua, F., You, Q., Huang, Q., Fu, W., & Zhou, X. (2024). Exploring guided wave propagation in composite cylindrical shells with an embedded delamination through refined spectral element method. *Thin-Walled Structures, 194*, Article 111326. doi:10.1016/j.tws.2023.111326

Karakoti, A., Pandey, S., & Kar, V. R. (2022). Nonlinear transient analysis of porous P-FGM and S-FGM sandwich plates and shell panels under blast loading and thermal environment. *Thin-Walled Structures, 173*, Article 108985. doi:10.1016/j.tws.2022.108985

Le, H. K., Bui, P. G., Do, C. Q., & Dang, H. V. (2022a). Buckling analysis of FG porous truncated conical shells resting on elastic foundations in the framework of the shear deformation theory. *Advances in Applied Mathematics and Mechanics, 14*(1), 218-247. doi:10.4208/aamm.OA-2020-0202

Le, H. K., Pham, H. V., Bui, H. T. T., & Do, C. Q. (2022b). Nonlinear buckling and postbuckling of ES-FG porous cylindrical shells under external pressure. *Modern Mechanics and Applications*, 743-754. doi:10.1007/978-981-16-3239-6_57

Li, H., Pang, F., Du, Y., & Gao, C. (2019). Free vibration analysis of uniform and stepped functionally graded circular cylindrical shells. *Steel and Composite Structures, 33*(2), 163-180. doi:10.12989/scs.2019.33.2.163

Li, S. R., Fu, X.-H., & Batra, R. C. (2010). Free vibration of three-layer circular cylindrical shells with functionally graded middle layer. *Mechanics Research Communications, 37*(6), 577-580. doi:10.1016/j.mechrescom.2010.07.006

Liang, C., Yaw, Z., & Lim, C. W. (2023). Thermal strain energy induced wave propagation for imperfect FGM sandwich cylindrical shells. *Composite Structures, 303*, Article 116295. doi:10.1016/j.compstruct.2022.116295

Liu, T., Wang, A., Wang, Q., & Qin, B. (2020). Wave based method for free vibration characteristics of functionally graded cylindrical shells with arbitrary boundary conditions. *Thin-Walled Structures, 148*, Article 106580. doi:10.1016/j.tws.2019.106580

Liu, Y., & Qin, Z. (2021). Nonlinear forced vibrations of FGM sandwich cylindrical shells with porosities on an elastic substrate. *Nonlinear Dyn, 104*(2), 1007-1021. doi:10.1007/s11071-021-06358-7

Love, A. E. H. (1888). XVI. The small free vibrations and deformation of a thin elastic shell. *Philosophical Transactions of the Royal Society of London, 179*, 491-546. doi:10.1098/rsta.1888.0016

Mellouli, H., Jrad, H., Wali, M., & Dammak, F. (2019). Meshless implementation of arbitrary 3D-shell structures based on a modified first order shear deformation theory. *Computers & Mathematics with Applications, 77*(1), 34-49. doi:10.1016/j.camwa.2018.09.010

Mindlin, R. (1951). Influence of rotatory inertia and shear on flexural motions of isotropic, elastic plates. *Journal of Applied Mechanics, 18*, 31-38. doi:10.1115/1.4010217

Mirjavadi, S. S., Forsat, M., Barati, M. R., & Hamouda, A. M. S. (2022). Geometrically nonlinear vibration analysis of eccentrically stiffened porous functionally graded annular spherical shell segments. *Mechanics Based Design of Structures and Machines, 50*(6), 2206-2220. doi:10.1080/15397734.2020.1771729

Najafizadeh, M. M., & Isvandzibaei, M. R. (2007). Vibration of functionally graded cylindrical shells based on higher order shear deformation plate theory with ring support. *Acta Mechanica, 191*, 75-91. doi:10.1007/s00707-006-0438-0

Punera, D., Kant, T., & Desai, Y. M. (2018). Thermoelastic analysis of laminated and functionally graded sandwich cylindrical shells with two refined higher order models. *Journal of Thermal Stresses, 41*(1), 54-79. doi:10.1080/01495739.2017.1373379

Qu, Y., Long, X., Yuan, G., & Meng, G. (2013). A unified formulation for vibration analysis of functionally graded shells of revolution with arbitrary boundary conditions. *Composites Part B: Engineering, 50*, 381-402. doi:10.1016/j.compositesb.2013.02.028

Ramteke, P. M., & Panda, S. K. (2023). Nonlinear thermomechanical static and dynamic responses of bidirectional porous functionally graded shell panels and experimental verifications. *Journal of Pressure Vessel Technology, 145*(4), Article 41301. doi:10.1080/17455030.2022.2058710

Shahbaztabar, A., Izadi, A., Sadeghian, M., & Kazemi, M. (2019). Free vibration analysis of FGM circular cylindrical shells resting on the Pasternak foundation and partially in contact with stationary fluid. *Applied Acoustics, 153*, 87-101. doi:10.1016/j.apacoust.2019.04.012

Sobhy, M. (2016). An accurate shear deformation theory for vibration and buckling of FGM sandwich plates in hygrothermal environment. *International Journal of Mechanical Sciences, 110*, 62-77. doi:10.1016/j.ijmecsci.2016.03.003

Sofiyev, A. H. (2011). Thermal buckling of FGM shells resting on a two-parameter elastic foundation. *Thin-Walled Structures, 49*(10), 1304-1311. doi:10.1016/j.tws.2011.03.018

Su, Z., & Jin, G. (2016). Vibration analysis of coupled conical-cylindrical-spherical shells using a Fourier spectral element method. *Journal of the Acoustical Society of America, 140*(5), 3925-3940. doi:10.1121/1.4967853

Tahir, S. I., Tounsi, A., Chikh, A., Al-Osta, M. A., Al-Dulaijan, S. U., & Al-Zahrani, M. M. (2022). The effect of three-variable viscoelastic foundation on the wave propagation in functionally graded sandwich plates via a simple quasi-3D HSDT. *Steel and Composite Structures, 42*(4), 501-511. doi:10.12989/scs.2022.42.4.501

Talebi, S., Hedayati, R., Sadighi, M., & Ashoori, A. R. (2022). Dynamic thermal buckling of spherical porous shells. *Thin-Walled Structures, 172*, Article 108737. doi:10.1016/j.tws.2021.108737

Timesli, A. (2021). Analytical modeling of buckling behavior of porous FGM cylindrical shell embedded within an elastic foundation. *Gazi University Journal of Science, 35*(1), 148-165. doi:10.35378/gujs.860783

Tornabene, F. (2009). Free vibration analysis of functionally graded conical, cylindrical shell and annular plate structures with a four-parameter power-law distribution. *Computer Methods in Applied Mechanics and Engineering, 198*(37/40), 2911-2935. doi:10.1016/j.cma.2009.04.011

Tornabene, F., Fantuzzi, N., & Bacciocch, M. (2014). Free vibrations of free-form doubly-curved shells made of functionally graded materials using higher-order equivalent single layer theories. *Composites Part B: Engineering, 67*, 490-509. doi:10.1016/j.compositesb.2014.08.012

Trabelsi, S., Zghal, S., & Dammak, F. (2020). Thermo-elastic buckling and post-buckling analysis of functionally graded thin plate and shell structures. *Journal of the Brazilian Society of Mechanical Sciences and Engineering, 42*(5), 1-22. doi:10.1007/s40430-020-02314-5

Vu, L. T., & Hoang, T. V. (2022a). Buckling behavior of thick porous functionally graded material toroidal shell segments under external pressure and elevated temperature including tangential edge restraint. *Journal of Pressure Vessel Technology, 144*(5), Article 51310. doi:10.1115/1.4053485

Vu, L. T., & Hoang, T. V. (2022b). Thermo-torsional buckling and postbuckling of thin FGM cylindrical shells with porosities and tangentially restrained edges. *Mechanics Based Design of Structures and Machines, 51*(12), 1-20. doi:10.1080/15397734.2022.2084752

Wang, X., Lu, G., & Xiao, D. G. (2002). Nonlinear thermal buckling for local delamination near the surface of laminated cylindrical shell. *International Journal of Mechanical Sciences, 44*(5), 947-965. doi:10.1016/S0020-7403(02)00028-0

Wu, S., Qu, Y., & Hua, H. (2013). Vibrations characteristics of joined cylindrical-spherical shell with elastic-support boundary conditions. *Journal of Mechanical Science and Technology, 27*(5), 1265-1272. doi:10.1007/s12206-013-0207-7

Xue, Y., Jin, G., Zhang, C., Han, X., & Chen, J. (2023). Free vibration analysis of functionally graded porous cylindrical panels and shells with porosity distributions along the thickness and length directions. *Thin-Walled Structures, 184*. doi:10.1016/j.tws.2022.110448

Zghal, S., Frikha, A., & Dammak, F. (2017). Static analysis of functionally graded carbon nanotube-reinforced plate and shell structures. *Composite Structures, 176*, 1107-1123. doi:10.1016/j.compstruct.2017.06.015

Zhang, S., Wang, M., Chen, C., Shahsavari, D., Karami, B., & Tounsi, A. (2022). Wave propagation in carbon nanotube-reinforced nanocomposite doubly-curved shells resting on a viscoelastic foundation. *Waves in Random and Complex Media*, 1-24. doi:10.1080/17455030.2022.2058710